INORGANIC CHEMISTRY

FRONTIERS

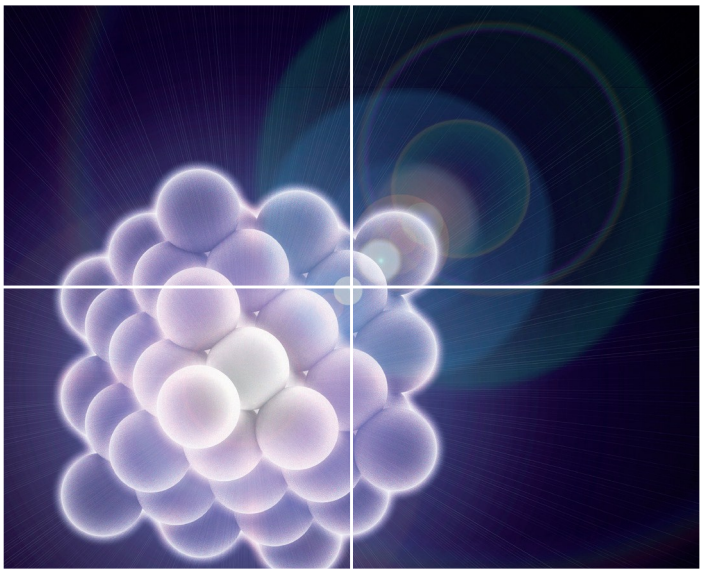

Accepted Manuscript

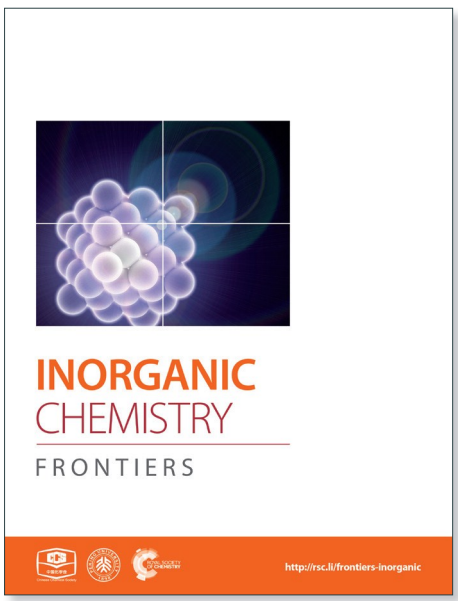

This is an *Accepted Manuscript*, which has been through the Royal Society of Chemistry peer review process and has been accepted for publication.

Accepted Manuscripts are published online shortly after acceptance, before technical editing, formatting and proof reading. Using this free service, authors can make their results available to the community, in citable form, before we publish the edited article. We will replace this *Accepted Manuscript* with the edited and formatted *Advance Article* as soon as it is available.

You can find more information about *Accepted Manuscripts* in the **Information for Authors**.

Please note that technical editing may introduce minor changes to the text and/or graphics, which may alter content. The journal's standard **Terms & Conditions** and the **Ethical guidelines** still apply. In no event shall the Royal Society of Chemistry be held responsible for any errors or omissions in this *Accepted Manuscript* or any consequences arising from the use of any information it contains.

Inorganic Chemistry Frontiers

ARTICLE

Functionalization of reduced graphene oxide with axially-coordinated metal-porphyrins: facile syntheses and temporally-dependent optical properties

Received 00th January 20xx,
Accepted 00th January 20xx

DOI: 10.1039/x0xx00000x

www.rsc.org/

Aijian Wang[a,c], Jingbao Song[a], Ding Jia[a], Wang Yu[a], Lingliang Long[a], Yinglin Song[b], Marie P. Cifuentes[d], Mark G. Humphrey[d], Long Zhang[c], Jianda Shao[c], and Chi Zhang[a,c]*

Reduced graphene oxide-tin porphyrin (RGO-SnTPP) nanohybrids with good dispersibility have been prepared by two covalent functionalization approaches. The microscopic structure and morphology of the RGO-SnTPP nanohybrids were characterized by various spectroscopic techniques including Fourier transform infrared spectroscopy, Raman spectroscopy, transmission electron microscopy, thermogravimetric analysis and X-ray photoelectron spectroscopy. Ground-state absorption and steady-state fluorescence studies indicate considerable π-π interactions and effective photo-induced electron and/or energy transfer from the porphyrin moieties to the RGO. Their nonlinear optical properties were investigated using the Z-scan technique at 532 nm with both picosecond and nanosecond laser pulses. The RGO-SnTPP hybrids were found to exhibit large nonlinear optical responses due to a combination of mechanisms, while significant differences in their nonlinear optical responses were observed, highlighting the influence on photophysical properties of the degree of functionalization and the synthetic approach employed.

Introduction

Porphyrins and related molecules have potential as modifiers to improve the physical and chemical properties of graphene, and are currently being actively explored as multipurpose innovative materials for optoelectronics application, as well as artificial photosynthetic building units.[1-3] Novel optoelectronic materials may result from strong electronic interactions between porphyrins and graphene, either from close proximity or from connection through conjugating units.[4-6] The utility of porphyrin/graphene nanohybrids that may exhibit optoelectronic functions strongly depends on the extent of the graphene dispersion and the strength of the interfacial adhesion. Although porphyrin/graphene nanocomposites can be obtained by noncovalent approaches,[7] an appropriate chemical treatment of the graphene surfaces is needed for a fine dispersion to be effected. In response to this requirement, the surface properties of graphene have been modified by the grafting of organic molecules to improve the dispersibility and compatibility, and thereby provide an efficient route to composite materials exhibiting unique combinations of functionalities superior to their constituents.[2,5]

Thus far, reports of graphene-based materials are largely restricted to graphene oxide (GO), which has chemically reactive oxygen functionalities, including carboxyl, epoxy, and hydroxyl groups; however, it is electrically insulating due to the disrupted sp^2 bonding network, and is therefore unfavorable for the construction of optoelectronic devices.[8,9] The electrical conductivity and electron transfer properties of graphene can be partially recovered on proceeding from GO to reduced graphene oxide (RGO), the key reduction step restoring the π network. Grafting organic moieties onto the surface of RGO can proceed with retention of the structural integrity of the RGO framework, thereby eliminating the problematic loss of electronic structure.[10] Chemical functionalization may therefore potentially pave the way for the use of RGO in practical applications. However, few reports have investigated the covalent chemical modification of RGO compared to the numerous reports of functionalization of GO, perhaps due to the reduced solubility of the former in the absence of electrostatic or steric protection, rendering further processing more difficult.[11] It is therefore of significant interest to design and prepare RGO-based solution-processed organic materials for further applications.

Some GO- and porphyrin-based nanohybrids with excellent optoelectronic properties have been reported,[4-6] but as yet, there has been no report of axially functionalized porphyrin-RGO nanohybrid materials. Encouraged by these considerations, we report herein two covalent functionalization approaches for the fabrication of RGO-TPP nanohybrid materials. These are based on the initial covalent introduction of phenol groups onto the RGO surfaces by 1,3-

[a] China-Australia Joint Research Center for Functional Molecular Materials, School of Chemical and Material Engineering, Jiangnan University, Wuxi 214122, P. R. China. E-mail: chizhang@jiangnan.edu.cn, Fax: (+86)-510-85917763
[b] School of Physical Science and Technology, Soochow University, Suzhou 215006, P. R. China
[c] Key Laboratory of Materials for High-Power Laser, Shanghai Institute of Optics and Fine Mechanics, Chinese Academy of Sciences, Shanghai 201800, P. R. China
[d] Research School of Chemistry, Australian National University, Canberra, ACT 2601, Australia

†Electronic Supplementary Information (ESI) available: See DOI: 10.1039/x0xx00000x

ARTICLE

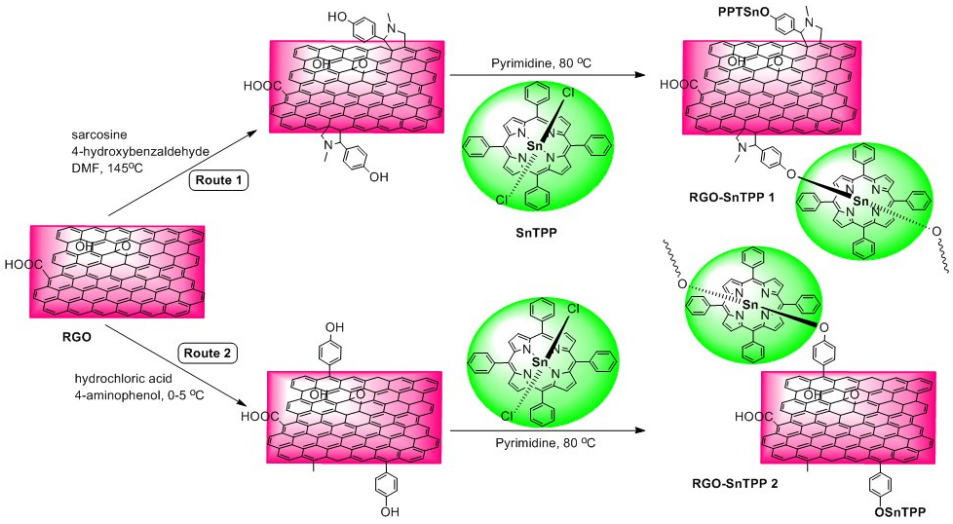

Scheme 1. Syntheses of RGO-SnTPP **1** and RGO-SnTPP **2**.

dipolar cycloaddition or a diazotization reaction, and subsequent nucleophilic substitution at dichloro(5,10,15,20-tetraphenylporphyrinato)tin(IV) (SnTPP). This covalent grafting of RGO with porphyrin is aimed at optimizing the RGO dispersion and enhancing interfacial bonding. The nanohybrid materials thus prepared are stable in solution and have been characterized by a variety of physical and spectral techniques. We have also explored the potential of combining porphyrin and RGO in a composite material to achieve increased nonlinear optical (NLO) activity. To the best of our knowledge, this is the first report of the fabrication and study of the photophysical and NLO properties of RGO nanohybrids covalently functionalized by axially-coordinated metal-porphyrins.

Results and Discussion

Syntheses: Several chemical procedures have been developed to functionalize graphene by covalent attachment of organic functional groups.[12] One of the main purposes of this functionalization is to improve the ease of dispersion of graphene in common solvents, which is a crucial step towards the formation of graphene-containing nanohybrid materials. More importantly, covalent functionalization of graphene with organic functional groups (such as chromophores) may combine the unique properties of each component while overcoming the dispersion shortcomings.[13-15] Although graphene is fairly inert, 1,3-dipolar cycloadditions and free radical reactions can provide efficient protocols for the functionalization of its sp^2 carbon framework, either thermally or by photophysical means.[16] Proposed by Prato and coworkers,[17] 1,3-dipolar cycloadditions permit the covalent functionalization of exfoliated graphene by in-situ-generated azomethine ylides, thereby incorporating fused pyrrolidines onto the skeleton of graphene; this procedure has been used extensively for the chemical modification of fullerenes[18] and carbon nanotubes,[19] with applications in various fields. Amongst the possible free radical reactions, the aryl diazonium reaction is a particularly efficient route to graphene functional-

Figure 1. Photographic image of the samples dispersed in DMSO (from left to right: RGO, RGO-SnTPP **1**, and RGO-SnTPP **2**).

ization. This versatile covalent reaction allows the preparation of self-tailored functional materials by simply changing the substituents in the benzene ring.[20] Both reactions have shown potential as key intermediate steps, facilitating post-functionalization of the graphene carbon network via solvent-assisted techniques.[21] Based on the foregoing considerations, we herein demonstrate two possible routes toward functionalizing RGO with axially-coordinated porphyrins (SnTPP), following 1,3-dipolar cycloadditions and free radical reactions. The preparative routes are shown in Scheme 1. The 1,3-dipolar cycloaddition was performed using sarcosine and 4-hydroxybenzaldehyde, both of which are commercially available. After reaction, most of the physically adsorbed organic materials were removed by filtration. The key outcome from this procedure is that hydroxyl groups can be grafted onto the RGO surfaces in a single reaction without degrading the resultant material's electronic properties, and this facile grafting in turn promotes a high grafting density of SnTPP. The phenol-functionalized RGO (Route 1) was then treated with SnTPP in dried pyridine under reflux to introduce the porphyrin moieties to the surface of RGO (RGO-SnTPP **1** in Scheme 1). Following aryldiazonium treatment of chemically reduced graphene, phenol groups were successfully immobilized on the solid surface (the reaction of

aryldiazonium with RGO was rigorously controlled). Subsequent grafting of SnTPP to the surface of RGO then followed via a straightforward nucleophilic substitution, affording the desired RGO-SnTPP **2** nanohybrid (Route 2). The two nanohybrids have greatly improved solubility compared to RGO (Figure 1), ascribed to the covalent linkage and π-π interactions between RGO and SnTPP.

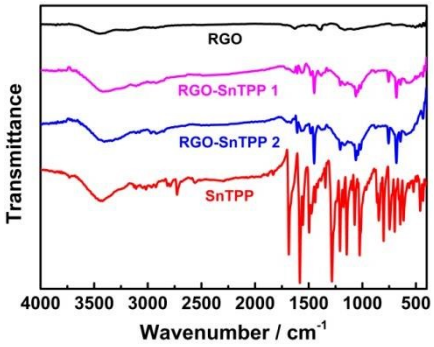

Figure 2. FTIR spectra of RGO, SnTPP and derivatized RGO (RGO-SnTPP **1** and RGO-SnTPP **2**).

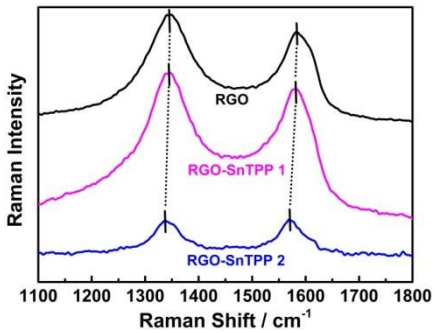

Figure 3. Raman spectra of pristine RGO, RGO-SnTPP **1** and RGO-SnTPP **2** (excitation wavelength 532 nm).

Characterization: FTIR spectra were employed to characterize the two forms of porphyrin-functionalized graphene.[22] The spectrum of pristine RGO is essentially featureless, indicating that most of the oxygen-containing functional groups in GO are removed following reduction (Figure 2). The chemical treatment with porphyrins via the different routes gives rise to the appearance of a number of characteristic bands, mainly in the spectral range of 400-1750 cm^{-1}. The major FTIR bands were assigned to characteristic fundamental vibrations of the functional groups, consistent with successful introduction of porphyrin molecules onto the RGO nanosheets. Comparing RGO-SnTPP **1** and RGO-SnTPP **2** with SnTPP, the small shift in the major band positions together with the significant changes in the intensities of the respective bands imply the presence of weak interactions of porphyrin moieties with RGO. Although the FTIR spectrum of RGO-SnTPP **1** displays bands that are very similar to those of RGO-SnTPP **2**, some differences between the spectra of the RGO-TPP nanohybrids were found, ascribed to the effect of the different synthetic routes and different resultant materials.

The Raman spectrum of RGO displays the typically strong tangential resonance absorption band (G band) at 1583 cm^{-1} and the defect band (D band) at 1349 cm^{-1} (Figure 3). The former has been used to estimate the level and distribution of modifications, while the latter has been employed to assess the density of defects and has been used to monitor the covalent functionalization which transforms sp^2 to sp^3 sites.[23] The D and G bands of RGO-SnTPP **1** appear at 1346 and 1581 cm^{-1}, respectively, shifted to slightly lower wavenumbers compared to RGO. In contrast, there is a significant shift to lower energy for the D (1349 to 1337 cm^{-1}) and G bands (1583 to 1569 cm^{-1}) of RGO-SnTPP **2** when compared to the analogous bands in the spectrum of RGO. Functionalization of graphene can result in enhancement of the D to G band intensity ratio (I_D/I_G).[24] In the present case, the SnTPP molecules grafted onto the RGO nanosheets contain a large number of sp^2 aromatic carbon atoms. Consequently, although some sp^2 carbon atoms in RGO were transformed to sp^3 carbon atoms, the numbers are still less than those of the sp^2 carbon atoms in the grafted porphyrins, leading to an overall decrease of the intensity ratio (I_D/I_G) from 1.15 for RGO to 1.12 for RGO-SnTPP **1** and 0.96 for RGO-SnTPP **2**, and consistent with a conjugated polymer-covalently grafted RGO functional material.[23] The Raman spectra of the RGO-SnTPP nanohybrids display similar modifications, but to different degrees. We have not found clear evidence of any Raman peaks characteristic of the functionalizing moieties, which may be due to either the low level of functionalization or random orientation of the SnTPP appendages rendering the direct detection of moieties on RGO exceedingly difficult. Their effect on the properties of RGO is abundantly clear, however. A simple method has been proposed, i.e., La (nm) = $(2.4 \times 10^{-10}) \times \lambda^4_{laser}(I_D/I_G)$ (where La represents the crystallite size and λ_{laser} is the laser excitation wavelength), which allows one to indirectly assess the density of graphene defects in terms of the crystallite size.[25] Based on the data in Figure 4, three sizes were obtained (22.1, 21.5 and 18.4 nm), corresponding to pristine RGO, RGO-SnTPP **1** and RGO-SnTPP **2**, respectively. The defect density of RGO-SnTPP **2** is larger (corresponding to a reduced crystallite size) than RGO and RGO-SnTPP 1. Indeed, the smaller size of the RGO-SnTPP nanohybrids compared to those of RGO can be directly observed (Figure 4). The existence of small nanoparticles distributed on the sheets of

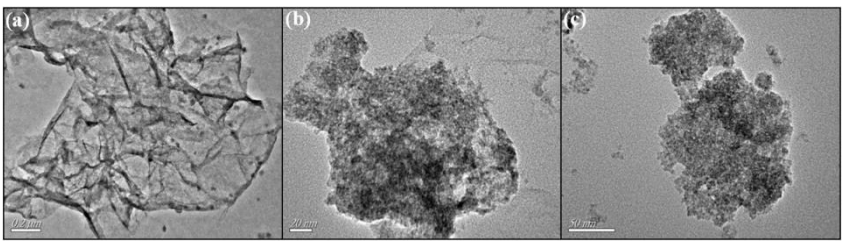

Figure 4. TEM images (on carbon-coated grids) of (a) RGO, (b) RGO-SnTPP **1**, and (c) RGO-SnTPP **2**.

RGO-SnTPP **1** and RGO-SnTPP **2** (Figures 4b and 4c) confirms the presence of SnTPP, and further supports the presence of covalent bonding between SnTPP and RGO.

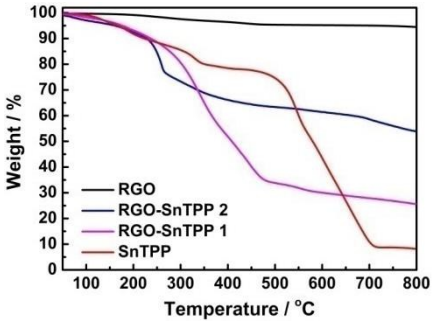

Figure 5. TGA profiles of RGO, SnTPP, RGO-SnTPP **1** and RGO-SnTPP **2** measured in nitrogen (heating rate 10 °C/min).

TGA characterization was also performed, to assess the thermal stability of the materials. TGA plots of RGO, SnTPP, RGO-SnTPP **1** and RGO-SnTPP **2** are shown in Figure 5. All samples were exhaustively washed and dried beforehand. RGO displays a weight loss of around 5% between 50 and 800 °C due to the removal of the residual oxygen functionalities, consistent with the reported results that RGO exhibits a similarly good thermal stability as that of pristine graphite.[26] Both RGO-SnTPP nanohybrids show some weight loss, consistent with the successful functionalization of RGO by axially-coordinated porphyrins. The thermal stability of RGO-SnTPP **2** is higher than that of RGO-SnTPP **1**. At 800 °C, the amount of the RGO-SnTPP **2** residue is 54%, whereas the amount of RGO-SnTPP **1** residue is 26%, both of which are significantly larger than SnTPP (8%) due to the presence of RGO. The TGA results display a good agreement with the XPS results (Figure 6), further indicating that the surfaces of the RGO nanosheets are coated with different amounts of porphyrin as a result of employing the two different synthetic routes.

XPS was examined to further investigate the chemical bonding at the surface of RGO following modification, the results being shown in Figure 6. Only two main peaks, corresponding to the carbon and oxygen species, are observed in the spectrum of RGO (Figure 6a). After functionalization with porphyrins, the spectra of RGO-SnTPP **1** and RGO-SnTPP **2** exhibited four new peaks, corresponding to Cl 2p, N 1s, Sn $3d_{3/2}$ and Sn $3d_{5/2}$ (Figure 6a), which confirms the formation of porphyrin grafted RGO.[27] Peaks of RGO-SnTPP **1** corresponding to Sn $3d_{3/2}$ and Sn $3d_{5/2}$ were observed at 495.0 and 486.3 eV. Due to the different chemical environments following functionalization, the binding energies of Sn $3d_{5/2}$ and Sn $3d_{3/2}$ in RGO-SnTPP **2** are blue-shifted by 0.2 eV and red-shifted by 0.3 eV, respectively (Figure 6b). The compositions of the RGO-SnTPP nanohybrids were also determined from the XPS results. The weight fractions of Sn in the samples of RGO-SnTPP **1** and RGO-SnTPP **2** were calculated to be 9.77% and 6.39%, respectively, based on which the SnTPP content in the nanohybrids can be determined to be 59.65% and 39.02%, which indicates that the porphyrin content in the two RGO-SnTPP nanohybrids declines on proceeding from RGO-SnTPP **1** to RGO-SnTPP **2** due to the different functionalization procedures.

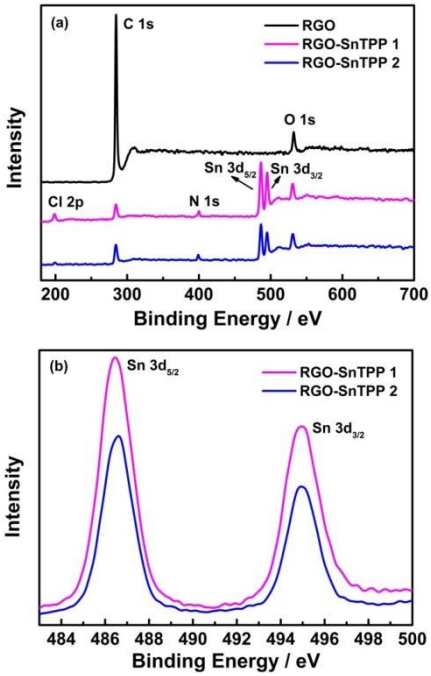

Figure 6. (a) XPS survey scans of RGO, RGO-SnTPP **1** and RGO-SnTPP **2**, and (b) XPS spectra of RGO-SnTPP **1** and RGO-SnTPP **2** in the regions of Sn $3d_{3/2}$ and Sn $3d_{5/2}$.

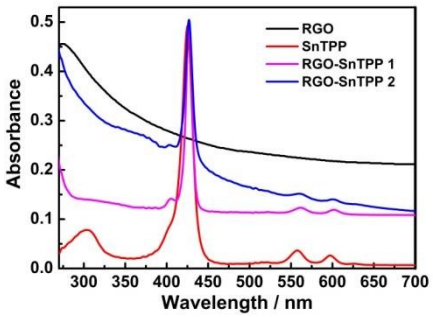

Figure 7. Ground-state absorption spectra of RGO, SnTPP, RGO-SnTPP **1** and RGO-SnTPP **2** in DMSO.

Photophysical properties: Porphyrins interact with various carbon materials through π-stacking between their electron-abundant aromatic cores and the conjugated surfaces of the carbon materials.[15,28,29] Similar interactions, which can be identified from ground-state absorption spectroscopy, are expected to occur between graphene and porphyrins (Figure 7). The absorption spectrum of RGO shows a strong broad absorption that decreases in intensity continuously to 700 nm. The absorption bands of the porphyrin-containing species are slightly broadened and red shifted in proceeding from free SnTPP to RGO-SnTPP **1** and then RGO-SnTPP **2**, the peaks shifting from 425 to 427 and then 428 nm, respectively, consistent with the presence of ground-state electronic and π-π interactions between SnTPP and RGO. In

addition, the relative intensity of the Soret band of the RGO-SnTPP nanohybrids is markedly reduced compared to that of SnTPP. However, the overall intensity of the porphyrin-centered transitions increases in proceeding from RGO-SnTPP **2** to RGO-SnTPP **1**, corresponding to the effect of the different synthetic routes and a consequent different degree of functionalization.

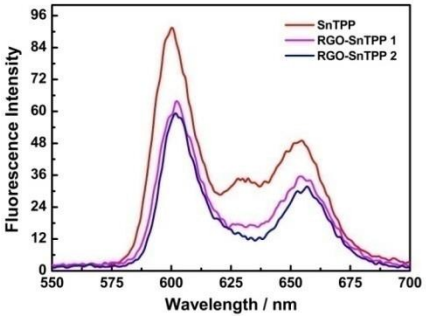

Figure 8. Fluorescence spectroscopic changes observed for SnTPP, RGO-SnTPP **1** and RGO-SnTPP **2** in DMSO upon excitation at 425 nm, with the normalization of the absorbance of the Soret band to the same value (0.51).

With the aim of probing the excited-state electronic interactions of porphyrin moieties and RGO, the fluorescence spectra of SnTPP, RGO-SnTPP **1** and RGO-SnTPP **2** were measured. The fluorescence spectrum of SnTPP undergoes modification following covalent functionalization at RGO (Figure 8), with Stokes shifts of 173 (SnTPP), 177 (RGO-SnTPP **1**), and 176 nm (RGO-SnTPP **2**). Electron movement through graphene is close to ballistic at room temperature,[30,31] so the Stokes shift in the hybrid system, resulting from the energy loss during the process from S_0-S_1 transition absorption to S_1-S_0 transition emission, is therefore less than that of SnTPP. Because RGO does not exhibit a fluorescence signal, the fluorescence of both RGO-SnTPP nanohybrids must be from the porphyrin moieties, which unequivocally confirms the presence of the porphyrin units. Furthermore, the fluorescence intensities of RGO-SnTPP **2** and RGO-SnTPP **1** clearly decrease in the order SnTPP **>** RGO-SnTPP **1 >** RGO-SnTPP **2**. This indicates that the quenching of the porphyrin moieties emission in RGO-SnTPP **2** is more effective than that in RGO-SnTPP **1**. Experimental results and molecular orbital theory have demonstrated that, due to its unique π-electron systems, RGO is a favorable electron acceptor when directly connected to an appropriate electron donor.[32] In RGO covalently linked SnTPP nanohybrid materials, the donor-acceptor interactions between RGO and SnTPP may involve two competitive processes: photo-induced electron and energy transfer from SnTPP to RGO,[32] and energy absorbing and electron transporting antenna-like behavior at SnTPP, which could result in fluorescence quenching and energy release. The observed red-shift in the emission maximum for RGO-SnTPP **2** and RGO-SnTPP **1** compared to SnTPP may be ascribed to the confinement of organic dye molecules on the surface of RGO and their interactions with the RGO nanosheets, which reflects the modification of the electronic state of SnTPP induced by RGO as demonstrated in the ground-state absorption spectra. The RGO can provide an ideal network to promote charge transfer in porphyrin-based systems and transport electrons to the collecting surface.

Nonlinear optical properties: The nonlinear optical (NLO) properties of materials are important for applications such as optical limiting, optical processing, and optical switching.[33,34] As a consequence, these properties has been widely investigated using several experimental techniques over the past years. The Z-scan technique is a sensitive method to characterize the NLO properties of materials with a simple experimental setup.[35] In the Z-scan technique, the sample moves along the beam propagating direction (z-axis) through the focus of a lens, and as it moves the sample is under variable irradiance. The total transmittance through the sample is recorded as a function of incident laser intensity at each z-position and analyzed using Z-scan theory.

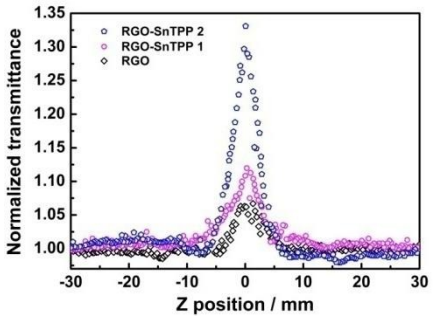

Figure 9. Open-aperture Z-scan traces of RGO, RGO-SnTPP **1** and RGO-SnTPP **2** in DMSO, obtained under 21 ps, 532 nm laser excitation.

In the present work, an open-aperture Z-scan experiment was used to investigate the NLO responses of RGO and the RGO-porphyrin nanohybrids (RGO-SnTPP **1** and RGO-SnTPP **2**) in both the picosecond (ps) and nanosecond (ns) regimes. The ps Z-scan was performed at an excitation wavelength of 532 nm with a 21 ps pulse width, while the ns measurements were carried out at 532 nm with a pulse width of 4 ns. In Figure 9, the open-aperture Z-scan traces of RGO, RGO-SnTPP **1** and RGO-SnTPP **2** using ps laser pulses are displayed. At the excitation wavelength, all samples exhibit clear saturable absorption responses; that is, the total transmission increases as the sample moves to the higher irradiance at the focal plane. A saturable absorption trace arises when the rate of generation of excited states is equal to the rate of their depletion by stimulated emission and excited relaxation.[36] The three samples can therefore effectively suppress low intensity light but allow higher intensity light to pass. For RGO nanosheets, the observed saturable absorption can be ascribed to a relatively slow decay process maintaining occupancy of the conduction band, with further photo-excited electrons being prevented from promotion to this band by Pauli blocking: two photo-excited electrons cannot occupy the same state because of the Pauli exclusion principle.[37] Thus, at the focal point, the intensity reaches a maximum, resulting in the observed saturable absorption. In these Z-scan traces, the saturable absorption signal increases on proceeding from RGO to RGO-SnTPP **1** and then RGO-SnTPP **2**, with the increased absorption a consequence of the covalent linkage between RGO and the porphyrins, and the results indicating that the saturable absorption can be tuned by varying the synthetic routes, which is in good agreement with the experimental results of thin films containing metallophthalocyanine chlorides.[38,39] The RGO-SnTPP nanohybrids are superior to RGO as saturable absorbers in the ps regime due to both the increased saturable absorption and the improved solubility and dispersion stability. Interestingly, this is in sharp contrast to the

nonlinear absorption performance of a different GO-SnTPP nanohybrid upon excitation at 532 nm with 21 ps pulses;[24] under the latter conditions, the GO-SnTPP nanohybrid exhibits an effective reverse saturable absorption behavior at the focal point, although the differing sample concentrations render comparison with the present study necessarily cautious.

There is currently considerable interest in using carbon nanotube-based nanohybrids as saturable absorbers.[40-42] The optical properties of the RGO-based nanohybrids in this work compare favorably with those of solid poly(methylmethacrylate) (PMMA) composites containing porphyrin-covalently-functionalized multi-walled carbon nanotubes (MWCNT-TPP) and of MWCNT-TPP in DMF;[43] specifically, the saturable absorption performance of our nanohybrids is superior to the MWCNT-TPP/PMMA composites and the MWCNT-TPP nanohybrid. However, any further comments are not justified, given the differences in experimental conditions such as wavelength, pulse width, repetition rate, etc.

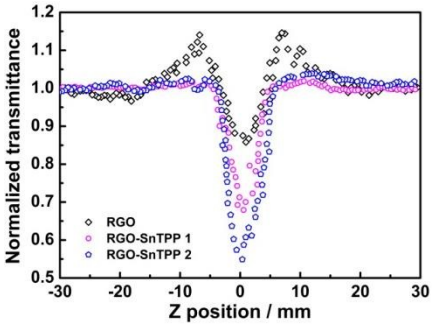

Figure 10. Open-aperture Z-scan traces of RGO, RGO-SnTPP **1**, and RGO-SnTPP **2** in DMSO, obtained under 4 ns, 532 nm laser excitation.

To gain a deeper insight into the nonlinear absorption responses, open-aperture Z-scan measurements were also performed at 532 nm with nanosecond laser pulses. As shown in Figure 10, the normalized transmittance curve of RGO exhibits two weaker shoulder peaks along with a valley, corresponding to a transformation from saturable absorption to reverse saturable absorption as the sample moves to the focus of a lens.[31] At low input fluence, the saturable absorption originating from Pauli blocking dominates the nonlinear absorption due to the state filling of the interband transitions in the sp^2-clusters.[44] The excited-state absorption arising from numerous localized sp^2 configurations in RGO dominates the nonlinear absorption at high input fluence, resulting in the observed nonlinear absorptive valley.[45] For other samples, a dip in the transmission appears at the focus (Figures 10 and S7), signaling the occurrence of reverse saturable absorption and hence optical limiting behavior.[46] The two RGO-SnTPP nanohybrids are superior at optical limiting to SnTPP, RGO and the control sample (blended RGO and SnTPP) (Figures 10 and S7). A similar result has been observed for host-guest systems such as cobalt phthalocyanine/DNA-CTMA (hexadecyltrimethylammonium chloride) surfactant complex and cobalt phthalocyanine/liquid crystals, which exhibited increased NLO properties compared with their precursors due to increases in charge-transfer effects.[47] The normalized transmittance of RGO-SnTPP **1** at the focal point, where the input fluence is a maximum, dropped to 67% of the incident intensity, identical within experimental error to the decrease to 66% for a previously-reported graphene nanohybrid covalently functionalized by zinc phthalocyanine.[48] However, the RGO-SnTPP **2** exhibits a much deeper valley, suggesting that RGO-SnTPP **2** possesses superior optical limiting performance. These nanohybrids therefore offer an easy way to tailor the NLO properties by judicious choice of the synthetic approach. The RGO-SnTPP nanohybrids have smaller nonlinear absorption responses than the porphyrin/Nafion based nanocomposites in Ref. [49], but different mechanisms are believed to be responsible for the observed NLO behavior of the RGO-SnTPP systems and the porphyrin/Nafion based nanocomposites, rendering further comments unwarranted.

The two-photon absorption coefficients β_2 for the nanohybrids, RGO, SnTPP, and the RGO/SnTPP blend were calculated by extrapolating the observed performance to neat material, assuming no contribution from the solvent (Table S1; as the molecular weights of all but SnTPP are unknown, it is not possible to compare the molecular two-photon absorption cross-sections σ_2).While being mindful of the errors associated with these measurements, it is clear that the β_2 values increase on proceeding from the components RGO and SnTPP to the nanohybrids, and that the β_2 values of the nanohybrids under ns conditions differ significantly from that of the RGO/SnTPP blend.

The improved NLO response can have contributions from various mechanisms such as excited-state absorption, nonlinear scattering and photo-induced electron or energy transfer. With organic dyes, NLO performance can be observed using long excitation pulses due to the radiative lifetimes of the lowest triplet states being sufficiently long that there is a corresponding population build-up in the triplet states.[50] In the present case, on excitation with nanosecond laser pulses, the intersystem crossing rate and triplet state lifetime of the porphyrin are significant, resulting in a reverse saturable absorption process. The nanohybrid functionalization may result in the small localized sp^2 environments increasing significantly in number, but not interconnecting to form new sp^2 carbon clusters in the RGO moiety,[51,52] as displayed in Scheme 1 and confirmed by the results of Raman, resulting in the improved excited-state absorption.[31] Knowledge of the nature of the nonlinear optical response, as well as the impact of the energy/electron transfer on nonlinearity, is very important;[53] in the present case, the photo-induced electron or energy transfer process between porphyrin and RGO that was documented in the fluorescence analysis may also contribute to the nonlinear absorption by fluorescence quenching and energy release.[54] Nonlinear scattering is often the strongest contributor to nonlinear absorption in nanomaterials. Work by Li et al suggests that nonlinear scattering is strongly connected to the thermal conductivity of graphene-based materials.[55] In the scattering process, the high intensity laser is dispersed, affording a beam with larger spatial dimensions, and thereby resulting in reduced intensity.[56] Effective nonlinear scattering can be observed on the nanosecond time scale, while the efficiency of scattering is largely dependent on the scattering cross-section, and hence the size of the scatterers.[34]

Based on the saturable absorption and reverse saturable absorption performance of the RGO-SnTPP nanohybrids, we anticipate that several novel RGO-based devices could be eventually realized through the use of concepts from the already

well-developed RGO optics research. (1) Attachment of the porphyrin moieties onto the surface of the RGO significantly improves the solubility and ease of processing of these RGO-porphyrin covalently functionalized materials. (2) The improved saturable absorption and reverse saturable absorption render RGO-TPP-related materials suitable for potential applications in ultrafast optical switching, as mode-locking elements, or as optical limiters for nanosecond pulses. (3) The work function of RGO is controlled by the chemical functionalization (and indeed the different synthetic routes), so one can expect such functionalization to lead to the control, tuning and tailoring of the NLO properties of RGO. It may also enable the generation of RGO-based optical devices, which may be comparable to, if not better than, the traditional optical materials.

Conclusions

RGO nanohybrids covalently modified with metal-porphyrins have been prepared by two synthetic routes, and found to possess improved NLO properties compared to those of their precursors, a result ascribed to the close interactions between RGO and porphyrins. The structural properties of the porphyrin-functionalized RGO nanohybrids were comprehensively characterized by using spectroscopic and electron microscopy techniques. Photophysical studies demonstrated considerable π-π interactions and effective photo-induced electron and/or energy transfer from the porphyrin moieties to the RGO. The nanohybrids displayed superior NLO performance to that of a RGO suspension at 532 nm under both picosecond and nanosecond regimes. The present research provides an effective approach to control the photophysical properties of RGO-based materials; the RGO-SnTPP hybrid materials may be competitive candidates for optical switching and optical limiting applications in optoelectronic devices due to their easy preparation, good solubility/processability and excellent optoelectronic properties.

Experimental Section

Materials: All reactions and manipulations were carried out under a nitrogen atmosphere with the use of standard Schlenk techniques. Pyridine and other organic solvents were dried and distilled before use. Unless otherwise noted, all reagents were purchased from commercial suppliers and used as received. Ultrapure water was used throughout this study. RGO and SnTPP were prepared according to reported procedures.[57,58]

Structure, morphology and composition characterization methods: The structure, microstructure and composition of the nanohybrids were characterized using various techniques. Raman spectra were obtained using a Renishaw inVia Raman Microscope with 532 nm laser excitation, and an exposure time of 50 seconds. Characteristic fundamental vibrations of the functional groups and confirmation of the presence of specific interactions between RGO and SnTPP were obtained from Fourier transform infrared (FTIR) spectra. The FTIR spectra were measured using a MB154S-FTIR spectrometer (Canada) with an Attenuated Total Reflectance device of resolution 4 cm^{-1} between 400 and 4000 cm^{-1}. The morphology and microstructural analysis of the hybrids were performed employing transmission electron microscopy (TEM). The chemical nature and elemental composition of RGO and its composites were characterized by X-ray photoelectron spectroscopy (XPS), which was performed on a RBD upgraded PHI-5000C ESCA (PerkinElmer) electron spectrometer with a Mg Kα line at 280 eV. Thermal analysis was run on a PerkinElmer Pyris 1 system from 50 to 800 ^{o}C under a N_2 purge and with a heating rate of 10 °C/min.

Ground-state absorption and steady-state fluorescence measurements: The ground-state absorption spectra of the samples were recorded in the range 200-700 nm using a UV/vis spectrophotometer (JASCO V-570) with DMSO as the solvent and a path length of 1 cm. A spectrofluorometer (Fluoro-Max-P) was used to record the steady-state fluorescence spectra. Samples were dissolved in dry DMSO (the absorbance of the Soret band is 0.51), transferred to a long quartz cell, and then capped and deoxygenated by sparging with N_2 before measurement (excitation wavelength 425 nm).

Nonlinear optical measurements: Z-scan measurements were carried out employing a Q-switched Nd:YAG laser with 4 ns and 21 ps pulses at 532 nm, and a repetition rate of 2 Hz. The laser beam was focused by a 30 cm focusing lens, after spatially removing higher-order modes. To facilitate comparison, all sample concentrations were adjusted to 0.15 mg/mL; all samples were examined in a 2 mm thick quartz cell. Two pyroelectric energy probes were used to monitor the input fluence and the fluence of the transmitted beam at regular intervals, as the sample was translated along the propagation direction of the focused Gaussian beam.

1,3-Dipolar cycloaddition at RGO to afford RGO-SnTPP 1: RGO (40 mg) and 4-hydroxybenzaldehyde (160 mg) were sonicated for 30 min in DMF (50 mL), and the reaction mixture was then heated at 145 ^{o}C with magnetic stirring. Sarcosine (800 mg) was added in portions (200 mg every 24 h) over a period of 5 days. The dark homogeneous mixture was added to water, affording a precipitate. The precipitate was collected with a 0.45 μm nylon membrane, and the solid was washed thoroughly with deionized water, methanol and ethanol until the washing solvent was clear, affording the 4-hydroxybenzaldehyde-functionalized RGO hybrid as a black solid (50 mg). The synthetic procedure for RGO-SnTPP **1** is shown in Scheme 1 (Route 1). SnTPP (100 mg) was added in portions (25 mg every 24 h) over a period of 5 days to a refluxing solution containing 4-hydroxybenzaldehyde-functionalized RGO (43 mg) in pyridine (20 mL). The reaction mixture was then cooled and centrifuged, and the solid was washed to remove excess reactants and finally freeze-dried under reduced pressure for 24 h, to give 35 mg of RGO-SnTPP **1** as a black powder.

Diazotization reaction at RGO to afford RGO-SnTPP 2: The diazotization reaction of 4-aminophenol was performed so as to effect chemical grafting onto RGO via C-C coupling and afford RGO-TPP **2**, as shown in Scheme 1. A solution of sodium nitrite (510 mg) in 15 mL of deionized water was slowly added to 10 mL of a 36%～38% hydrochloric acid solution containing 4-aminophenol (500 mg) with stirring and the reaction temperature was maintained at 0-5 ^{o}C until the completion of reaction. The pH of the solution containing the previously sonicated RGO (40 mg) was adjusted to be slightly acidic (pH 6) by adding dilute HCl solution, while the solution was

maintained in an ice bath. The aryldiazonium ion solution was then added dropwise to the RGO solution. The reaction was maintained for 5 h at 0-5 ^{o}C and then at room temperature for another 19 h. The mixture was passed through a 0.45 μm nylon membrane. The filter cake thus obtained was washed with deionized water, ethanol and dilute hydrochloric acid until the filtrate was clear. The residual black solid was dried under vacuum to afford 4-aminophenol-functionalized RGO. To prepare RGO-SnTPP **2**, 4-aminophenol-functionalized RGO (43 mg) was reacted with SnTPP (100 mg) in pyridine (20 mL) at reflux for 5 days while stirring. After the reaction, the work-up procedures for RGO-SnTPP **2** were as above for the RGO-SnTPP **1** hybrid material.

Acknowledgements

Financial support from the National Natural Science Foundation of China (51432006, 50925207, 51172100), the Ministry of Science and Technology of China for the International Science Linkages Program (2011DFG52970), the Ministry of Education of China for the Changjiang Innovation Research Team (IRT13R24), the Ministry of Education and the State Administration of Foreign Experts Affairs for the 111 Project (B13025), 100 Talents Program of CAS, and Jiangsu Innovation Research Team are gratefully acknowledged. M.G.H. and M.P.C. thank the Australian Research Council (ARC) for support.

Notes and references

1 M. O. Senge, M. Fazekas, E. G. A. Notaras, W. J. Blau, M. Zawadzka, O. B. Locos, E. M. N. Mhuircheartaigh, *Adv. Mater.* 2007, **19**, 2737.
2 V. Georgakilas, M. Otyepka, A. B. Bourlinos, V. Chandra, N. Kim, K. C. Kemp, P. Hobza, R. Zboril, K. S. Kim, *Chem. Rev.* 2012, **112**, 6156.
3 M. Drobizhev, Y. Stepanenko, A. Rebane, C. J. Wilson, T. E. O. Screen, H. L. Anderson, *J. Am. Chem. Soc.* 2006, **128**, 12432.
4 H. Xu, P. Wu, C. Liao, C. G. Lv, Z. Z. Gu, *Chem. Commun.* 2014, **50**, 8951.
5 Y. F. Xu, Z. B. Liu, X. L. Zhang, Y. Wang, J. G. Tian, Y. Huang, Y. F. Ma, X. Y. Zhang, Y. S. Chen, *Adv. Mater.* 2009, **21**, 1275.
6 M. B. M. Krishna, N. Venkatramaiah, R. Venkatesan, D. N. Rao, *J. Mater. Chem.* 2012, **22**, 3059.
7 Y. X. Xu, L. Zhao, H. Bai, W. J. Hong, C. Li, G. Q. Shi, *J. Am. Chem. Soc.* 2009, **131**, 13490.
8 P. V. Kamat, *J. Phys. Chem. Lett.* 2011, **2**, 242.
9 A. J. Wang, W. Yu, Z. G. Xiao, Y. L. Song, L. L. Long, M. P. Cifuentes, M. G. Humphrey, C. Zhang, *Nano Res.* 2015, **8**, 870.
10 B. Zhang, Y. Chen, G. Liu, L. Q. Xu, J. N. Chen, C. X. Zhu, K. G. Neoh, E. T. Kang, *J. Polym. Sci. A: Polym. Chem.* 2012, **50**, 378.
11 W. W. Tu, J. P. Lei, S. Y. Zhang, H. G. Ju, *Chem. Eur. J.* 2010, **16**, 10771.
12 V. Georgakilas, M. Otyepka, A. B. Bourlinos, V. Chandra, N. Kim, K. C. Kemp, P. Hobza, R. Zboril, K. S. Kim, *Chem. Rev.* 2012, **112**, 6156.
13 J. R. Lomeda C. D. Doyle, D. V. Kosynkin, W. F. Hwang, J. M. Tour, *J. Am. Chem. Soc.* 2008, **130**, 16201.
14 C. K. Chua, M. Pumera, *Chem. Soc. Rev.* 2013, **42**, 3222.
15 F. Bonaccorso, Z. Sun, T. Hasan, A. C. Ferrari, *Nat. Photonics* 2010, **4**, 611.
16 L. Rodríguez-Pérez, M. Á. Herranz, N. Martín, *Chem. Commun.* 2013, **49**, 3721.
17 M. Quintana, K. Spyrou, M. Grzelczak, W. R. Browne, P. Rudolf, M. Prato, *ACS Nano* 2010, **4**, 3527.
18 M. Maggini, G. Scorrano, M. Prato, *J. Am. Chem. Soc.* 1993, **115**, 9798.
19 D. Tasis, N. Tagmatarchis, A. Bianco, M. Prato, *Chem. Rev.* 2006, **106**, 1105.
20 E. Bekyarova, M. E. Itkis, P. Ramesh, C. Berger, M. Sprinkle, W. A. de Heer, R. C. Haddon, *J. Am. Chem. Soc.* 2009, **131**, 1336.
21 S. P. Economopoulos, N. Tagmatarchis, *Chem. Eur. J.* 2013, **19**, 12930.
22 G. C. Wei, M. M. Yan, R. H. Dong, D. Wang, X. Z. Zhou, J. F. Chen, J. C. Hao, *Chem. Eur. J.* 2012, **18**, 14708.
23 B. Zhang, G. Liu, Y. Chen, L. J. Zeng, C. X. Zhu, K. G. Neoh, C. Wang, E. T. Kang, *Chem. Eur. J.* 2011, **17**, 13646.
24 A. J. Wang, L. L. Long, W. Zhao, Y. L. Song, M. G. Humphrey, M. P. Cifuentes, X. Z. Wu, Y. S. Fu, D. D. Zhang, X. F. Li, C. Zhang, *Carbon* 2013, **53**, 327.
25 M. Fang, K. G. Wang, H. B. Lu, Y. L. Yang, S. Nutt, *J. Mater. Chem.* 2010, **20**, 1982.
26 J. F. Shen, Y. Z. Hu, M. Shi, X. Lu, C. Qin, C. Li, M. X. Ye, *Chem. Mater.* 2009, **21**, 3514.
27 Y. Deng, Y. J. Li, J. Dai, M. D. Lang, X. Y. Huang, *J. Polymer Sci. A: Polymer Chem.* 2011, **49**, 1582.
28 D. M. Guldi, *Chem. Soc. Rev.* 2002, **31**, 22.
29 D. Baskaran, J. W. Mays, P. Zhang, M. S. Bratcher, *J. Am. Chem. Soc.* 2005, **127**, 6916.
30 Z. Sun, T. Hasan, F. Torrisi, D. Popa, G. Privitera, F. Wang, F. Bonaccorso, D. M. Basko, A. C. Ferrari, *ACS Nano* 2010, **4**, 803.
31 W. N. Song, C. Y. He, W. Zhang, Y. C. Gao, Y. X. Yang, Y. Q. Wu, Z. M. Chen, X. C. Li, Y. L. Dong, *Carbon* 2014, **77**, 1020.
32 A. Wojcik, P. V. Kamat, *ACS Nano* 2010, **4**, 6697.
33 Q. L. Bao, H. Zhang, J. X. Yang, S. Wang, D. Y. Tang, R. Jose, S. Ramakrishna, C. T. Lim, K. P. Loh, *Adv. Funct. Mater.* 2010, **20**, 782.
34 X. L. Xu, W. W. Qiu, Q. Zhou, J. Tang, F. Yang, Z. R. Sun, P. Audebert, *J. Phys. Chem. B* 2008, **112**, 4913.
35 M. Sheik-Bahae, A. A. Said, T. H. Wei, D. J. Hagan, E. W. van Stryland, *IEEE J. Quantum Elect.* 1990, **26**, 760.
36 S. Zongo, M. S. Dhlamini, P. H. Neethling, A. Yao, M. Maaza, B. Sahraoui, *Opt. Mater.* 2015, **50**, 138.
37 Q. L. Bao, H. Zhang, Y. Wang, Z. H. Ni, Y. L. Yan, Z. X. Shen, K. P. Loh, D. Y. Tang, *Adv. Funct. Mater.* 2009, **19**, 3077.
38 A. Zawadzka, A. Karakas, P. Płóciennik, J. Szatkowski, Z. Lukasiak, A. Kapceoglu, Y. Ceylan, B. Sahraoui, *Dyes Pigments* 2015, **112**, 116.
39 A. Zawadzka, P. Płóciennik, J. Strzelecki, A. Korcala, A. K. Arof, B. Sahraoui, *Dyes Pigments* 2014, **101**, 212.
40 V. Scardaci, Z. P. Sun, F. Wang, A. G. Rozhin, T. Hasan, F. Hennrich, I. H. White, W. I. Milne, A. C. Ferrari, *Adv. Mater.* 2008, **20**, 4040.
41 F. Wang, A. G. Rozhin, V. Scardaci, Z. Sun, F. Hennrich, I. H. White, W. I. Milne, A. C. Ferrari, *Nat. Nanotech.* 2008, **3**, 738.
42 V. Scardaci, A. G. Rozhin, P. H. Tan, F. Wang, I. H. White, W. I. Milne, A. C. Ferrari, *Phys. Stat. Sol. B* 2008, **245**, 2319.
43 X. L. Zhang, Z. B. Liu, X. Zhao, X. Q. Yan, X. C. Li, J. G. Tian, *Opt. Express* 2013, **21**, 25277.
44 S. Muhammad, H. L. Xu, R. L. Zhong, Z. M. Su, A. G. Al-Sehemi, A. Irfan, *J. Mater. Chem. C* 2013, **1**, 5439.
45 G. K. Lim, Z. L. Chen, J. Clark, R. G. S. Goh, W. H. Ng, H. W. Tan, R. H. Friend, P. K. H. Ho, L. L. Chua, *Nat. Photonics* 2011, **5**, 554.
46 É. M. N. Mhuircheartaigh, S. Giordani, W. J. Blau, *J. Phys. Chem. B* 2006, **110**, 23136.
47 B. Derkowska, M. Wojdyla, W. Bala, K. Jaworowicz, M. Karpierz, J. G. Grote, O. Krupka, F. Kajzar, B. Sahraoui, *J. Appl. Phys.* 2007, **101**, 083112.
48 X. Zhao, X. Q. Yan, Q. Ma, J. Yao, X. L. Zhang, Z. B. Liu, J. G. Tian, *Chem. Phys. Lett.* 2013, **577**, 62.

49 M. Maaza, N. Mongwaketsi, M. Genene, G. Hailu, G. Garab, B. Sahraoui, D. Hamidi, *J. Porphyrin Phthalocyanine* 2012, **16**, 987.
50 S. Sreeja, S. Sreedhanya, N. Smijesh, R. Philip, C. I. Muneera, *J. Mater. Chem. C* 2013, **1**, 3851.
51 G. Eda, Y. Y. Lin, C. Mattevi, H. Yamaguchi, H. A. Chen, I. S. Chen, C. W. Chen, M. Chhowalla, *Adv. Mater.* 2010, **22**, 505.
52 C. Mattevi, G. Eda, S. Agnoli, S. Miller, K. A. Mkhoyan, O. Celik, D. Mastrogiovanni, G. Granozzi, E. Garfunkel, M. Chhowalla, *Adv. Funct. Mater.* 2009, **19**, 2577.
53 N. Mongwaketsi, S. Khamlich, M. Pranaitis, B. Sahraoui, F. Khammar, G. Garab, R. Sparrow, M. Maaza, *Mater. Chem. Phys.* 2012, **134**, 646.
54 Z. B. Liu, Y. F. Xu, X. Y. Zhang, X. L. Zhang, Y. S. Chen, J. G. Tian, *J. Phys. Chem. B* 2009, **113**, 9681.
55 X. J. Xu, D. X. Ou, X. L. Luo, J. Chen, J. J. Lu, H. B. Zhan, Y. Q. Dong, J. G. Qin, Z. Li, *J. Mater. Chem.* 2012, **22**, 22624.
56 C. Zheng, M. Feng, Y. H. Du, H. B. Zhan, *Carbon* 2009, **47**, 2889.
57 J. F. Shen, Y. Z. Hu, C. Li, C. Qin, M. X. Ye, *Small* 2009, **5**, 82.
58 M. J. Crossley, P. Thordarson, R. A. S. Wu, *J. Chem. Soc., Perkin Trans.* 2001, **1**, 2294.